

Application of Battery Storage to Switching Predictive Control of Power Distribution Systems Including Road Heating*

Chiaki Kojima¹, Yuya Muto², Hikaru Akutsu¹, Rinnosuke Shima¹, and Yoshihiko Susuki³

Abstract—A road heating system is an electrical device which promotes snow melting by burying a heating cable as a thermal source underground. When integrating road heating into the power distribution system, we need to optimize the flow of electric power by appropriately integrating distributed power sources and conventional power distribution equipment. In this paper, we extend the power distribution system considered in the authors' previous study to the case where battery storage is installed. As a main result, we propose a predictive switching control that achieves the reduction of distribution loss, attenuation of voltage fluctuation, and efficient snow melting, simultaneously. We verify the effectiveness of the application of battery storage through numerical simulation.

I. INTRODUCTION

In heavy snowfall regions, there has long been a serious problem of great inconvenience and danger to people's lives, for example falling on sidewalks, heavy workload due to snow removal, traffic congestion and etc [1][2]. A road heating system is one of the electrical devices which promotes snow melting by burying a thermal source underground, and raises the temperature of the ground surface [3]. However, the road heating system consumes a large amount of electrical power when we integrate road heating into the power distribution system [4][5]. We need to optimize the flow of electrical power by properly integrating distributed power sources, e.g. photovoltaic power generation (PV), and electric vehicles (EVs) with conventional power distribution equipment for an appropriate operation of power distribution systems.

Against the problem explained in the above paragraph, the authors of this paper [6] have derived a mathematical model of the power distribution system including road heating, and of snowmelting on the ground surface via thermal diffusion in the underground based on the nonlinear ordinary differential equation (ODE) model [7][8]. Furthermore, the authors proposed a predictive control by switching of the power distribution system including road heating [9]. The proposed control of [9] achieves reduction of power distribution losses, attenuation of voltage impact, and efficient snowmelting, simultaneously. However, the supply of power

*This work was supported by Azbil Yamatake General Foundation and JSPS KAKENHI Grant Numbers 20K04552, 23K03910.

¹Chiaki Kojima, Hikaru Akutsu, and Rinnosuke Shima are with Department of Electrical and Electronic Engineering, Faculty of Engineering, Toyama Prefectural University, 5180, Kurokawa, Imizu, Toyama, 939-0398, Japan chiaki@pu-toyama.ac.jp

²Yuya Muto is with Department of Electrical and Computer Engineering, Graduate School of Engineering, Toyama Prefectural University, 5180, Kurokawa, Imizu, Toyama, 939-0398, Japan

³Department of Electrical Engineering, Graduate School of Engineering, Kyoto-Daigaku-Katsura, Nishikyo-ku, Kyoto 615-8510, Japan

electricity from the PV power generation equipment is limited to the distribution system only. There is a potential for improvement in terms of power flow optimization.

Based on the considerations given in the above paragraph, the purpose of this paper is to extend the results of the previous study [9] in the following two points.

- We introduce a switching to the PV power generation equipment to achieve a more efficient power distribution system operation which does not depend on transmission from the grid.
- A battery storage is introduced to the considered power distribution system to make effective use of surplus power generated by PV in the past.

Based on the above extension, this paper improves the optimization of power flow by applying the battery storage to the power distribution system, making more efficient use of the available power from the PV power generation equipment and the battery storage. As a main result, we give a design of predictive switching control of the distribution system under study, as well as a design of predictive control of the PV power generation equipment and battery storage. Finally, we verify the effectiveness of these predictive controls through numerical simulations. Through this verification, we show that the predictive control of the distribution system is more efficient than the previous study [9].

The outline of this paper is described as follows. In Section II, we introduce a mathematical model of a power distribution system including road heating. As a main result, we give a switching predictive control for the system based on an evaluation function to simultaneously achieve reduction of distribution losses, attenuation of voltage impact, and efficient snowmelting in Section III. Finally, we verify an effectiveness of the proposed switching predictive control via numerical simulation in Section IV.

II. MODELING OF POWER DISTRIBUTION SYSTEM

In this section, we develop the distribution system including road heating considered in a previous study due to the authors [6][9] to a mathematical model for the case including switching of the discharging of PV power generation equipment and battery storage.

A. Overall setup of system

In this subsection, we describe the overall setup of the power distribution system including road heating. We show an overview of the system in Fig. 1. In the system, electrical power is supplied from the underground power distribution lines to the load electrical equipment (residences, EVs,

lamps, and etc.) and from the PV electric power generation equipment to the underground power distribution lines. Assuming a realistic burial location, a heating cable is buried in parallel with the underground power distribution line in the horizontal direction. Two switches are connected at both terminals to control the voltage distribution over the heating cable. When Switch 1 is turned On, the power electricity is transmitted from the starting end of the heating cable. On the other hand, the power is transmitted from the battery storage if Switch 2 is turned On. In addition, the heat generated in the cable of the distribution line is transferred within the cable, and diffused into the underground. The Joule heat propagating to the ground surface is used to melt snow.

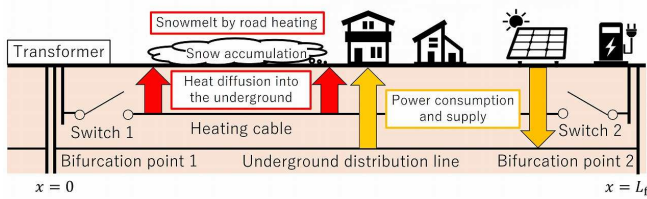


Fig. 1. Considered power distribution system

We show a single-line diagram of the power distribution system in Fig. 2. The branches of the underground power distribution line and the heating cable at the starting point and terminal are denoted as Bifurcation points 1 and 2, respectively. We assume that Transformers A and B are connected to Switches 1 and 2, respectively.

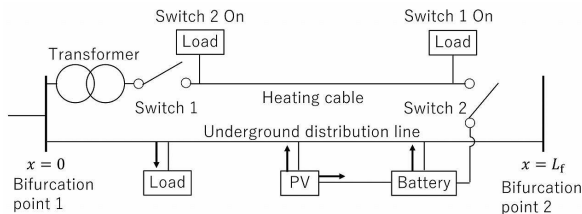


Fig. 2. Single-line diagram of the considered power distribution system

B. Voltage distribution on underground power distribution line [7][8]

We consider the three-phase underground power distribution line where the line extends in a straight line from the transformer to the load electrical equipment and PV electric generation equipment between both bifurcation points as shown in Fig. 2. We also suppose that there are no voltage regulation devices such as transformers on the intermediate positions over the lines. The horizontal spatial variable on the underground power distribution line is defined as x [m]. The starting point and terminal of the line correspond to $x = 0$ [m] and $x = L_f$ [m], $L_f > 0$, respectively.

1) *Voltage distribution on underground power distribution line:* We describe the voltage distribution of an underground power distribution line, which is assumed to be in three-phase equilibrium, by the ordinary differential equations with

position x [m] as an independent variable, for an arbitrarily fixed time t [min]. We denote the voltage phasor for single-phase at position x and time t by $v_e(x; t)e^{j\theta_e(x; t)}$, where j is the imaginary unit. Then, $\theta_e(x; t)$ [rad] and $v_e(x; t)$ [V] correspond to the voltage phase and amplitude, respectively. The spatial variation on the distribution voltage profile is described by the nonlinear ODE model [7][8]:

$$\frac{d\theta_e(x; t)}{dx} = -\frac{s_e(x; t)}{v_e(x; t)^2},$$

$$\frac{dv_e(x; t)}{dx} = w_e(x; t),$$

$$\frac{ds_e(x; t)}{dx} = \frac{b_e p_e(x, t) - g_e q_e(x, t)}{g_e^2 + b_e^2}, \quad (1)$$

$$\frac{dw_e(x; t)}{dx} = \frac{s_e(x; t)^2}{v_e(x; t)^3} - \frac{g_e p_e(x, t) + b_e q_e(x, t)}{(g_e^2 + b_e^2)v_e(x; t)}, \quad (2)$$

where $s_e(x, t)$ [V^2/m] and $w_e(x, t)$ [V/m] represent the supplemental variable and voltage gradient at position x and time t , respectively. In (1) and (2), $p_e(x, t)$ [W/m] and $q_e(x, t)$ [Var/m] are active and reactive powers at position x and time t of the underground power distribution line, respectively. If $p_e(x, t) > 0$ holds, $p_e(x, t)$ denotes the active power, i.e. the supply, flowing to the distribution line at x . On the other hand, if $p_e(x, t) < 0$ holds, $p_e(x, t)$ corresponds to the active power consumption flowing from the line at x . The same inequality holds for the reactive power $q_e(x, t)$. Due to the assumptions made at the terminal of the underground power distribution line, $p_e(L_f, t) = 0$ and $q_e(L_f, t) = 0$ hold. The constants g_e [S/m] and b_e [S/m] are the conductance and susceptance per unit length at position x of the line. Since the distribution loss $\Gamma_e(x; t)$ [W/m] of the underground distribution line is considered for three phases, the distribution loss for a single-phase is three times larger, and is given by

$$\Gamma_e(x; t) = 3g_e \left(w_e(x; t)^2 + \frac{s_e(x; t)^2}{v_e(x; t)^2} \right)$$

from [12].

2) *Boundary condition:* The voltage phase and amplitude satisfy the following boundary conditions at each point:

$$\text{Bifurcation point 1: } \theta_e(0, t) = \theta_1, \quad v_e(0, t) = v_1, \quad (3)$$

$$\text{Bifurcation point 2: } \theta_e(L_f, t) = \theta_2(t), \quad v_e(L_f, t) = v_2(t), \quad (4)$$

In (3), θ_1 and v_1 denote the voltage phase and amplitude in Bifurcation point 1, respectively, which are supposed to be constant. Moreover, $\theta_2(t)$ and $v_2(t)$ are the voltage phase and amplitude in Bifurcation point 2 at time t , respectively, in (4).

C. Voltage and temperature distribution of heating cable [6]

We assume that the heating cable is single-phase two-wire system. The heating cable extends in a straight line from Transformer A to Transformer B with the switches connected at both ends. The horizontal spatial variable of the heating cable is x [m] in common with underground

power distribution line. The vertical spatial variable y [cm] is the depth from the ground surface to the heating cable. This implies that $y = 0$ [cm] and $y = D_f$ [cm] correspond to the ground and the surface, respectively.

1) *Voltage distribution*: We denote the voltage phasor for single-phase at position x and time t by $v_h(x; t)e^{j\theta_h(x; t)}$, where $\theta_h(x; t)$ [rad] and $v_h(x; t)$ [V] are the voltage phase and amplitude, respectively. Similarly to the underground power distribution line, the spatial variation of the voltage distribution over the heating cable, which is assumed to be single-phase two-wire system, is described by the nonlinear ODE model [6].

$$\frac{d\theta_h(x, t)}{dx} = -\frac{s_h(x, t)}{v_h(x, t)^2},$$

$$\frac{dv_h(x, t)}{dx} = w_h(x, t),$$

$$\frac{ds_h(x, t)}{dx} = \frac{b_h p_h(x, t) - g_h q_h(x, t)}{g_h^2 + b_h^2}, \quad (5)$$

$$\frac{dw_h(x, t)}{dx} = \frac{s_h(x, t)^2}{v_h(x, t)^3} - \frac{g_h p_h(x, t) + b_h q_h(x, t)}{(g_h^2 + b_h^2)v_h(x, t)}, \quad (6)$$

where $s_h(x, t)$ [V²/m] and $w_h(x, t)$ [V/m] represent the supplemental variable and voltage gradient at position x and time t , respectively. In (5) and (6), $p_h(x, t)$ [W/m] and $q_h(x, t)$ [Var/m] are active and reactive powers at position x and time t of the heating cable, respectively. These powers satisfy the same properties that described for the underground power distribution line in the previous section. Moreover, g_h [S/m] and b_h [S/m] are the conductance and susceptance per unit length at position x of the cable, respectively.

2) *Setting of transformers*: We define $\theta_o(t)$ [rad], $v_o(t)$ [V], $s_o(t)$ [V²], and $w_o(t)$ [V/m] as the voltage phase, voltage amplitude, supplemental variable, and voltage gradient of Transformer o ($o = A, B$). At Transformer A, $\theta_A(t) = \theta_A$ and $v_A(t) = v_A$ are supposed to be constant. The turn ratio corresponds to the transformation ratio of the voltage amplitudes. The following equalities hold at each transformer from [8]:

$$\text{Transformer A: } \theta_h(0, t) = \theta_A, \quad v_h(0, t) = \frac{1}{a_A} v_A,$$

$$s_h(0, t) = s_A(t), \quad w_h(0, t) = a_A w_A(t),$$

$$\text{Transformer B: } \theta_h(L_f, t) = \theta_B(t), \quad v_h(L_f, t) = \frac{1}{a_B} v_B(t),$$

$$s_h(L_f, t) = s_B(t), \quad w_h(L_f, t) = a_B w_B(t).$$

We describe the boundary conditions of the voltage phase and amplitude, supplemental variable, and voltage gradient at positions $x = 0$ and $x = L_f$ over the heating cable. The boundary conditions are described as follows corresponding

to the switching patterns:

Switches 1 and 2: Off:

$$\theta_h(0; t) = 0, \quad v_h(0; t) = 0, \quad s_h(0; t) = 0, \quad w_h(0; t) = 0,$$

$$\theta_h(L_f; t) = 0, \quad v_h(L_f; t) = 0, \quad s_h(L_f; t) = 0, \quad w_h(L_f; t) = 0,$$

Switch 1: On:

$$\theta_h(0; t) = \theta_1, \quad v_h(0; t) = \frac{1}{a_1} v_1,$$

$$s_h(L_f; t) = 0, \quad w_h(L_f; t) = 0,$$

Switch 2: On:

$$s_h(0; t) = 0, \quad w_h(0; t) = 0,$$

$$\theta_h(L_f; t) = \theta_1, \quad v_h(L_f; t) = \frac{1}{a_1} v_1.$$

In the above conditions, θ_1 [rad] and v_1 [V] denote the reference voltage phase and amplitude for the underground distribution line at $x = 0$. Moreover, a_1 is the transformer ratio of the single phase transformer.

3) *Thermal distribution of heating cable surface*: At the surface of the heating cable, the transient spatial and temporal variation of the temperature satisfies the following ODE:

$$\frac{d\delta_{\text{surf,diff}}(t; x)}{dt} = \frac{\Gamma_h(x, t) \times 10^{-2} - q_r - \gamma_{\text{cable}} \delta_{\text{surf,diff}}(t; x)}{C_{\text{cable}}}$$

from [10][11], where $\delta_{\text{surf,diff}}(t; x)$ [°C] is the difference of the temperature between the surface and the ambient surroundings. In addition, C_{cable} [J/cm·°C] is the heat capacity of the cable, q_r [W/cm] is the radiative cooling supposed to be constant, and γ_{cable} [W/m·K] is the contact heat transfer coefficient per unit length between the cable surface and soil. From [12], $\Gamma_h(t; x)$ [W/m] is the power distribution loss (Joule heat) of the heating cable at position x and time t

$$\Gamma_h(t; x) = g_h \left(w_h(t; x)^2 + \frac{s_h(t; x)^2}{v_h(t; x)^2} \right). \quad (7)$$

The cable surface temperature $\delta_{\text{surf}}(t; x)$ [°C] at position x and time t is given by $\delta_{\text{surf}}(t; x) = \delta_{\text{surf,diff}}(t; x) + \delta_{\text{soil}}(D_f, t; x)$, where $\delta_{\text{soil}}(D_f, t; x)$ [°C] is the temperature of the soil at position x and depth $y = D_f$. Based on the surface temperature and contact heat transfer [13], the boundary condition at the surface is given by

$$-\lambda_{\text{tran}} \frac{d\delta_{\text{soil}}(D_f, t; x)}{dy} = \beta_{\text{cable}} (\delta_{\text{surf}}(x, t) - \delta_{\text{soil}}(D_f, t; x)),$$

where λ_{tran} [W/m·K] and β_{cable} [W/m²·K] are the thermal conductivity of the soil and the heat transfer coefficient between heating cable and soil, respectively.

D. Switches

Since the voltages at Transformer B and the terminal ($x = L_f$) of the underground power distribution line are required to be equal, if one switch is On, the other switch is Off. Moreover, if the heating cable is not used, both switches are

Off. We define $\sigma_i(t) \in \{0, 1\}$ ($i = 0, 1, 2$) as the binary variable by

$$\begin{aligned}\sigma_0(t) &:= \begin{cases} 1 & (\text{Switches 1 and 2: Off}) \\ 0 & (\text{Otherwise}), \end{cases} \\ \sigma_1(t) &:= \begin{cases} 1 & (\text{Switch 1: On, Switch 2: Off}) \\ 0 & (\text{Otherwise}), \end{cases} \\ \sigma_2(t) &:= \begin{cases} 1 & (\text{Switch 1: Off, Switch 2: On}) \\ 0 & (\text{Otherwise}). \end{cases}\end{aligned}$$

These variables can be regarded as the control input to the power distribution system. We refer to the integer i as the index of the control input $\sigma_i(t)$.

We assume that the PV power generation equipment can transmit the generated electrical power to either underground power distribution line or battery storage. We define the binary variable $\sigma_{\text{pv}}(t) \in \{0, 1\}$ related to the power transmission for the equipment by corresponding to the direction of the power transmission as follows:

$$\sigma_{\text{pv}}(t) := \begin{cases} 1 & (\text{Underground distribution line}) \\ 0 & (\text{Battery storage}). \end{cases}$$

In the battery storage, it is assumed that the active power is supplied only from the PV power generation equipment. We assume that a certain amount of power can be transmitted to either the heating cable or the underground power distribution line, respectively. We also allow for the possibility of not transmitting power to either of them. The binary variable $\sigma_{\text{battery},i}(t) \in \{0, 1\}$ ($i = 0, 1, 2$) for the transmission of power from the battery storage is defined by the following equality corresponding to the direction of the power transmissions as the control input to the power distribution system:

$$\begin{aligned}\sigma_{\text{battery},0}(t) &:= \begin{cases} 1 & (\text{No power transmission}) \\ 0 & (\text{Otherwise}), \end{cases} \\ \sigma_{\text{battery},1}(t) &:= \begin{cases} 1 & (\text{Underground distribution line}) \\ 0 & (\text{Otherwise}), \end{cases} \\ \sigma_{\text{battery},2}(t) &:= \begin{cases} 1 & (\text{Heating cable}) \\ 0 & (\text{Otherwise}). \end{cases}\end{aligned}$$

E. Thermal Diffusion in Underground and Snow Volume [6]

1) *Thermal diffusion*: Throughout this paper, we assume that there is no horizontal thermal diffusion, and that the diffusion occurs only in the vertical direction in the underground. We define the underground temperature of the soil at position x , depth y and time t by $\delta_{\text{soil}}(y, t; x)$ [$^{\circ}\text{C}$]. The spatial and temporal variation of the temperature is described by the following standard thermal conduction equation:

$$\frac{\partial \delta_{\text{soil}}(y, t; x)}{\partial t} = \alpha_{\text{soil}} \frac{\partial^2 \delta_{\text{soil}}(y, t; x)}{\partial y^2},$$

where α_{soil} [m^2/s] is thermal diffusivity of soil, respectively. The boundary condition at the ground surface is given by

the thermal conduction equation with the thermal exchange from the snow accumulation [13]:

$$-\lambda_{\text{tran}} \frac{d\delta_{\text{soil}}(0, t; x)}{dy} = \beta_{\text{ground}}(\delta_{\text{soil}}(0, t; x) - \delta_{\text{snow}}),$$

where β_{ground} [$\text{W}/\text{m} \cdot \text{K}$] is the contact heat transfer coefficient per unit length between the ground surface and accumulation of snow. Moreover, δ_{snow} [$^{\circ}\text{C}$] is the constant snow temperature on the ground surface.

2) *Snow melting*: We suppose that the snow melting occurs due to the radiant heat from the sunlight and the Joule heat of the heating cable for simplicity. The spatial and temporal variation of the snow volume $h_{\text{snow}}(x, t)$ [mm] is described by the following equation [14]:

$$\frac{dh_{\text{snow}}(t; x)}{dt} = -\frac{a_{\text{snow}}}{d_{\text{snow}}}(\mu_1(x, t) + \mu_2(x, t)) + f_{\text{snow}}(t). \quad (8)$$

where $h_{\text{snow}}(x, t)$ [mm] is the snow volume and $f_{\text{snow}}(t)$ [mm/min] is the snowfall per 1 minute. Moreover, d_{snow} [g/cm^3] is the density of snow volume, and a_{snow} is the unit conversion factor from the unit W/m^2 to the unit mm/min. Finally, $\mu_1(x, t)$ [W/m^2] represents the snowmelting due to the sunlight at position x and time t . The snowmelting due to the influence of the sunlight is given by $\mu_1(x, t) = \phi_r(t) + \phi_s(x, t) + \phi_l(x, t)$, where $\phi_r(t)$ [W/m^2] is the net radiation flux at time t , which is assumed to be independent on position x . Moreover, $\phi_s(x, t)$ [W/m^2] and $\phi_l(x, t)$ [W/m^2] denote the sensible and latent heat fluxes at position x and time t , respectively. In addition, $\mu_2(x, t)$ [W/m^2] represents the snowmelting due to the Joule heat of the cable at position x and time t . Finally, in (8), the snowmelting due to the Joule heat of the heating cable is expressed as $\mu_2(x, t) = \beta_{\text{ground}}(\delta_{\text{soil}}(0, t; x) - \delta_{\text{snow}})$.

III. SWITCHING PREDICTIVE CONTROL

In this section, we explain the predictive control by switches connected to the heating cables and the predictive control of the PV power generation equipment and the battery storage as the main results of this paper.

A. Design of Switching Predictive Control

In this subsection, we explain the overall process for the predictive switching control of the power distribution system, the PV power generation equipment, and predictive control of battery storage. The optimal control inputs are computed according to Steps 0-5 below. Note that Step 0 and Steps 1-4 correspond to the preliminary and during operation of the predictive control, respectively. We also add Steps 3 and 4 to the predictive switching control of the previous study [9] due to the authors of this paper.

- Step 0: We define the minimum switching time between the switching and the power transmission from the battery storage as T_{mini} [min]. Moreover, we define the predictive horizon as T_{pred} [min]. We prepare the time series data at each time $t = kT_{\text{mini}}$ ($k = 0, 1, 2, \dots$) for the residential load, PV power generation, solar radiation, snowfall, temperature, wind speed, and snow accumulation as inputs for the predictive simulation.

- **Step 1:** We define $N := \frac{T_{\text{pred}}}{T_{\text{mini}}}$ as the total number of times at which switching can occur. This number corresponds to the sum of all 3^N switching patterns, 2^N PV transmission patterns, and 3^N discharging patterns of the battery storage. For all possible $3^N + 2^N + 3^N$ patterns, we perform the simulations from $t = kT_{\text{mini}}$ to $t + T_{\text{pred}} = (k + N)T_{\text{mini}}$ based on the mathematical model of the distribution system.
- **Step 2:** Based on the simulation in Step 1, we compute the value of the evaluation function $J[k]$ for the possible 3^N switching patterns $\sigma_d[k]$ at $t = kT_{\text{mini}}$. We then compare the 3^N values of the functions. We choose the optimal switching pattern $\sigma_d^*[k]$ that has the smallest value at $t = kT_{\text{mini}}$. We explain the detailed procedure of the design of the optimal switching pattern in Section III-B.
- **Step 3:** Based on the simulation and the optimal switching pattern $\sigma_d^*[k]$ computed in Steps 1 and 2, respectively, we compute the evaluation function for the 2^N possible transmission patterns of the PV power generation equipment at $t = kT_{\text{mini}}$. We compute the value of the evaluation function $J_{\text{pv}}[k]$ for $\sigma_{\text{d,pv}}[k]$ of the transmission patterns of the PV power generation equipment at $t = kT_{\text{mini}}$. Then, by comparing the 2^N values of the evaluation functions, we find the optimal transmission pattern $\sigma_{\text{d,pv}}^*[k]$ of the PV power generation equipment whose value is the minimum at $t = kT_{\text{mini}}$. The detailed procedure of this step is explained in Section III-C.
- **Step 4:** Based on the predictive simulation in Step 1, the optimal switching pattern $\sigma_d^*[k]$ in Step 2, and the optimal transmission pattern $\sigma_{\text{d,pv}}^*[k]$ in Step 3, we compute the values of the evaluation function $J_{\text{battery}}[k]$ for the 3^N battery storage transmission pattern $\sigma_{\text{d,battery}}[k]$ at $t = kT_{\text{mini}}$ for the evaluation function $J_{\text{battery}}[k]$. In this case, the 3^N values of the evaluation function are compared, and the battery transfer pattern $\sigma_{\text{d,battery}}[k]$ with the minimum value at $t = kT_{\text{mini}}$ is selected as the optimal power transfer pattern $\sigma_{\text{d,battery}}^*[k]$. We explain the detailed procedure of the design of the optimal switching pattern in Section III-D.
- **Step 5:** For the optimal switching pattern and the optimal transmission pattern computed in the previous steps, the control inputs are continuously applied from $t = kT_{\text{mini}}$ to $t + T_{\text{mini}} = (k + 1)T_{\text{mini}}$. Then, we choose the switching pattern which has the smallest value of the evaluation function as the optimal switching pattern. Fig. 3 illustrates the overall flow of the switching and power transmission selection from Step 2 to Step 4.

B. Optimal Switching of Heating Cable

In this subsection, we give the evaluation function that determines the switching on the heating cable. We define the evaluation function $J[k]$ at $t = kT_{\text{mini}}$ by

$$J[k] := w_{\text{loss}} P_{\text{loss}}[k] + w_{\text{fluc}} V_{\text{fluc}}[k] + w_{\text{snow}} S_{\text{snow}}[k] + w_{\text{cost}} M_{\text{cost}}[k].$$

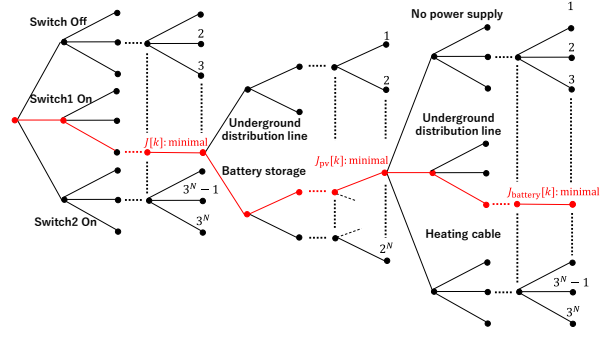


Fig. 3. Selection tree of switches

The exact definitions and physical meaning of each term are explained in the remainder of this section.

- **The first term:** The function $P_{\text{loss}}[k]$ [W·min] corresponds to the distribution loss of overall system in the time interval $[t, t + T_{\text{pred}}]$, and w_{loss} is the weighting coefficient corresponding the loss. This function is defined by the distribution loss of the underground power distribution line and heating cable:

$$P_{\text{loss}}[k] := \sum_{l=1}^N \int_{(k+l-1)T_{\text{mini}}}^{(k+l)T_{\text{mini}}} \int_0^{L_f} \Gamma(x; t) dx dt, \\ \Gamma(x; t) := \Gamma_e(x; t) + \Gamma_h(x; t). \quad (9)$$

In (9), $\Gamma_e(x; t)$ [W/m] and $\Gamma_h(x; t)$ [W/m] represent the distribution loss of the underground power distribution line and heating cable, respectively. Since the distribution loss of underground distribution line is considered for three phases, the distribution loss for a single-phase is three times larger and is given by

$$\Gamma_e(x; t) = 3g_e \left(w_e(x; t)^2 + \frac{s_e(x; t)^2}{v_e(x; t)^2} \right)$$

from [12], and $\Gamma_h(x, t)$ [W/m] is given by (7).

- **The second term:** The function $V_{\text{fluc}}[k]$ [V] corresponds to the evaluation of the voltage fluctuation of the underground power distribution line in the time interval $[t, t + T_{\text{pred}}]$, and w_{fluc} is the weighting coefficient in the evaluation of the fluctuation. The function $V_{\text{fluc}}[k]$ is defined by the maximum absolute values of the difference between the voltage amplitude and the reference value v_1 [V] for N intervals:

$$V_{\text{fluc}}[k] := \sum_{l=1}^N \max_{\tau \in ((k+l-1)T_{\text{mini}}, (k+l)T_{\text{mini}})} \max_{x \in [0, L_f]} |v_e(x; \tau) - v_1|. \quad (10)$$

- **The third term:** The function $S_{\text{snow}}[k]$ [m²·min] corresponds to the snow volume at all points in the time interval $[t, t + T_{\text{pred}}]$, and is defined by

$$S_{\text{snow}}[k] := \sum_{l=1}^N \int_{(k+l-1)T_{\text{mini}}}^{(k+l)T_{\text{mini}}} \int_0^{L_f} h_{\text{snow}}(x, t) dx dt,$$

where w_{snow} is the weighting coefficient in the evaluation of the volume.

- **The fourth term:** The function $M_{\text{cost}}[k]$ corresponds to the cost of operating the heating cable during the time interval $[t, t+T_{\text{pred}})$, and w_{cost} represents the weighting coefficient of its evaluation in the evaluation function. As we suppose that the owner of the heating cable, the PV power generation equipment, and the battery storage is supposed to be the same. the cost occurs only when Switch 1 is set to On. Thus, the cost $M_{\text{cost}}[k]$ is defined as

$$M_{\text{cost}}[k] := \sum_{l=1}^N \int_{(k+l-1)T_{\text{mini}}}^{(k+l)T_{\text{mini}}} m_{\text{cost}}(t) dt.$$

In the above equality, $m_{\text{cost}}(t)$ is defined by

$$m_{\text{cost}}(t) := \begin{cases} -p_{\text{h}}(x_{\text{load}}, t) & (\text{Switch 1: On}) \\ 0 & (\text{otherwise}), \end{cases}$$

where $p_{\text{h}}(x_{\text{load}}, t)$ [W/m], $p_{\text{h}}(x_{\text{load}}, t) \leq 0$ is the active power of the loads over the heating cable. Moreover, x_{load} corresponds to one of connection positions of the load on the heating cable except for the starting point $x = 0$ and the terminal $x = L_{\text{f}}$.

We define the discrete-time vector $\sigma_{\text{d}}[k]$, which consists of switching patterns from $t = kT_{\text{mini}}$ to $t + T_{\text{pred}} = (k + N)T_{\text{mini}}$, by

$$\sigma_{\text{d}}[k] := \begin{bmatrix} \sigma_{\text{d},0}[k] \\ \sigma_{\text{d},1}[k] \\ \sigma_{\text{d},2}[k] \end{bmatrix}, \quad \sigma_{\text{d},i}[k] := \begin{bmatrix} \sigma_{\text{d},i}[k] \\ \sigma_{\text{d},i}[k+1] \\ \vdots \\ \sigma_{\text{d},i}[k+N] \end{bmatrix} \quad (i = 0, 1, 2).$$

We enumerate all 3^N patterns $\sigma_{\text{d}}[k]$, and perform a numerical simulation for each of them. We obtain the optimal switching pattern $\sigma_{\text{d}}^*[k] \in \{0, 1\}^N$ at $t = kT_{\text{mini}}$ by solving the binary minimization problem

$$\sigma_{\text{d}}^*[k] = \underset{\sigma_{\text{d}}[k] \in \{0, 1\}^N}{\operatorname{argmin}} J[k].$$

From the current time $t = kT_{\text{mini}}$ to the next switching time $t + T_{\text{mini}} = (k + 1)T_{\text{mini}}$, we continue to apply the following optimal control input $\sigma_{\text{opt},i}(t)$ ($i = 0, 1, 2$) by

$$\sigma_{\text{opt},i}(t) = \sigma_{\text{d},i}^*(kT_{\text{mini}}), \quad t \in [kT_{\text{mini}}, (k + 1)T_{\text{mini}}).$$

C. Optimal Switching of PV Power Generation Equipment

In this subsection, we formulate the evaluation function that determines the destination of power electricity from the PV power generation equipment. Specifically, this function $J_{\text{pv}}[k]$ is mathematically defined by

$$J_{\text{pv}}[k] := w_{\text{pvfluc}} V_{\text{pvfluc}}[k] - w_{\text{stor},1} B_{\text{stor},1}[k].$$

- **The first term:** The function $V_{\text{pvfluc}}[k]$ [V] corresponds to the evaluation of the voltage fluctuation of the underground power distribution line in the time interval $[t, t + T_{\text{pred}})$, and w_{pvfluc} represents the weighting coefficient

in the evaluation function. The function $V_{\text{pvfluc}}[k]$ is defined in the same way as in the equation (10).

- **The second term:** The function $B_{\text{stor},1}[k]$ corresponds to the evaluation of the battery power in the time interval $[t, t + T_{\text{pred}})$, and $w_{\text{stor},1}$ is the weighting coefficient in the evaluation function. Since the owner of the PV power generation equipment and the battery storage are assumed to be the same, this function corresponds to smoothing for the amount of power electricity $P_{\text{battery}}(t)$ [kWh] of the battery storage. Thus, we define $B_{\text{stor},1}[k]$ to be large when the amount of power electricity in the battery storage is small. On the other hand, we set $B_{\text{stor},1}[k]$ to be small when the amount of power electricity in the battery storage is large. In this case, $B_{\text{stor},1}[k]$ can be defined by the following equality:

$$B_{\text{stor},1}[k] := \sum_{l=1}^N \int_{(k+l-1)T_{\text{mini}}}^{(k+l)T_{\text{mini}}} \zeta_{\text{stor},1}(t) dt,$$

where $\zeta_{\text{stor},1}(t)$ is defined as follows corresponding to the power transmissions:

$$\zeta_{\text{stor},1}(t) := \begin{cases} 0 & (\text{Underground power distribution line}) \\ \frac{1}{P_{\text{battery}}(t)} & (\text{Battery storage}). \end{cases}$$

We describe the design of the predictive control of PV power generation equipment. We define the vector consisting of the transmission patterns from time $t = kT_{\text{mini}}$ to $t + T_{\text{pred}} = k + NT_{\text{mini}}$ by

$$\sigma_{\text{d,pv}}[k] := \begin{bmatrix} \sigma_{\text{d,pv}}[k] \\ \sigma_{\text{d,pv}}[k+1] \\ \vdots \\ \sigma_{\text{d,pv}}[k+N] \end{bmatrix}.$$

We enumerate all 2^N possible transmission patterns $\sigma_{\text{d,pv}}[k]$, and compute the value of the evaluation function $J_{\text{pv}}[k]$ corresponding to each transmission pattern. Then, the optimal transmission pattern $\sigma_{\text{d,pv}}^*[k] \in \{0, 1\}^N$ is expressed as

$$\sigma_{\text{d,pv}}^*[k] = \underset{\sigma_{\text{d,pv}}[k] \in \{0, 1\}^N}{\operatorname{argmin}} J_{\text{pv}}[k].$$

During the time interval from time $t = kT_{\text{mini}}$ to the next switching time $t + T_{\text{mini}} = (k + 1)T_{\text{mini}}$, the control input $\sigma_{\text{opt,pv}}(t)$ is given by

$$\sigma_{\text{opt,pv}}(t) = \sigma_{\text{d,pv}}^*(kT_{\text{mini}}), \quad t \in [kT_{\text{mini}}, (k + 1)T_{\text{mini}}).$$

D. Optimal Discharging of Battery Storage

In this subsection, We provide an evaluation function that determines the destination of the power discharged from the battery storage. We define the evaluation function $J_{\text{battery}}[k]$ by

$$J_{\text{battery}}[k] := w_{\text{batteryfluc}} V_{\text{batteryfluc}}[k] + w_{\text{stor},2} B_{\text{stor},2}[k].$$

- **The first term:** The function $V_{\text{batteryfluc}}[k]$ [V] correspond to the evaluation of the voltage fluctuation of the

underground distribution line in the time interval $[t, t + T_{\text{pred}})$, and is defined in the same way as in the definition (10). Moreover, $w_{\text{batteryfluc}}$ is the weighting coefficient of its evaluation.

- **The second term:** The function

$$B_{\text{stor},2}[k] := \sum_{l=1}^N \int_{(k+l-1)T_{\text{mini}}}^{(k+l)T_{\text{mini}}} \zeta_{\text{stor},2}(t) dt$$

corresponds to the evaluation of the amount of electricity in battery storage in the time interval $[t, t + T_{\text{pred}})$, where $\zeta_{\text{stor},2}(t)$ is defined as follows corresponding to the power transmissions:

$$\zeta_{\text{stor},2}(t) := \begin{cases} \frac{1}{P_{\text{battery}}(t)} & \text{(Underground power distribution} \\ & \text{line or heating cable)} \\ 0 & \text{(No power transmission)} \end{cases}$$

In addition, $w_{\text{stor},2}$ represents the weighting coefficient of the evaluation.

We define the vector consisting of the discharging pattern from $t = kT_{\text{mini}}$ to $t = k + T_{\text{pred}} = k + NT_{\text{min}}$ by

$$\sigma_{\text{d,battery}}[k] := \begin{bmatrix} \sigma_{\text{d,battery},0}[k] \\ \sigma_{\text{d,battery},1}[k] \\ \sigma_{\text{d,battery},2}[k] \end{bmatrix},$$

$$\sigma_{\text{d,battery},i}[k] := \begin{bmatrix} \sigma_{\text{d,battery},i}[k] \\ \sigma_{\text{d,battery},i}[k+1] \\ \vdots \\ \sigma_{\text{d,battery},i}[k+N] \end{bmatrix} \quad (i = 0, 1, 2).$$

We enumerate all 3^N patterns of $\sigma_{\text{d,battery}}[k]$, and perform predictive simulations of the switching control. Then, the optimal discharging pattern $\sigma_{\text{d,battery}}^*[k] \in \{0, 1\}^N$ at $t = kT_{\text{mini}}$ is expressed as

$$\sigma_{\text{d,battery}}^*[k] = \underset{\sigma_{\text{d,battery}}[k] \in \{0,1\}^N}{\operatorname{argmin}} J_{\text{battery}}[k].$$

Then, during the time interval from $t = kT_{\text{mini}}$ to the next switching time $t + T_{\text{mini}} = (k+1)T_{\text{mini}}$, we continue to apply the optimal control input

$$\sigma_{\text{opt,battery},i}(t) = \sigma_{\text{d,battery},i}^*(kT_{\text{mini}}) \quad (i = 0, 1, 2),$$

$$t \in [kT_{\text{mini}}, (k+1)T_{\text{mini}}).$$

IV. NUMERICAL VERIFICATION

In this section, we verify the effectiveness of the proposed predictive switching control via numerical simulations considering two cases of typical power consumption, PV electric power generation, and weather conditions. These simulations suppose the winter season of Toyama Prefecture which is one of the heaviest snowfall areas in Japan.

A. Simulation Setting

In this subsection, we provide the setting of the power distribution system considered in the numerical simulation. We consider a power distribution system consisting of the underground power distribution line and the heating cable with length 100 m. The single-line diagram of the system is

illustrated in Fig. 4. For the underground power distribution line, the reference voltage amplitude for p.u. value is set to $v_1 = \frac{6600}{\sqrt{3}}$ [V]. Since we deal with only one of the three phases of the underground distribution line in this paper, we convert this reference value of line voltage $\sqrt{3}v_1 = 6600$ [V] to a phase voltage. In the heating cable, the reference voltage amplitude for the p.u. value is set to $\frac{1}{a_1}v_1 = 200$ [V], where $a_1 = \frac{33}{\sqrt{3}}$ is the transformer ratio. The load electrical equipment is installed at the horizontal position $x = 25$ [m] from Bifurcation point 1, and the PV electric power generation equipment is installed at $x = 50$ [m]. In addition, the battery storage is connected at $x = 75$ [m]. The connecting position x_{load} [m] of the load of the heating cable is given by

$$\begin{cases} \text{No load connected} & \text{(Switches 1 and 2: Off)} \\ x_{\text{load}} = L_f & \text{(Switch 1: On)} \\ x_{\text{load}} = 0 & \text{(Switch 2: On)}. \end{cases}$$

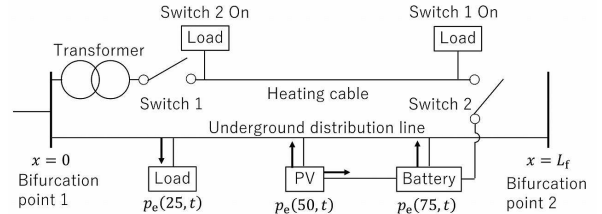


Fig. 4. Single-line diagram of power distribution system considered in numerical simulation

We describe the parameters used in the simulations of this section. The parameters related to the voltage distribution in the underground power distribution line and heating cable are shown in Tables I and II, respectively. For underground power distribution line and heating cable, the reference voltage amplitudes for the p.u. values are $v_1 = 6600$ [V] and $\frac{1}{a_1}v_1 = 200$ [V], respectively. We assume that no reactive power is supplied at all position x of the underground power distribution line and heating cable, i.e. $q_e(x, t) = q_h(x, t) = 0$ [p.u.]. The parameters related to the temperature distribution of the heating cable, the thermal diffusion in the underground, and the snowmelting on the ground surface are shown in Table III. The parameters related to the evaluation function are summarized in Table IV. We set the prediction horizon to be $T_{\text{pred}} = 30$ [min] from the viewpoint of the prediction of temporal changes of snow melting against the occurrence of pedestrian falls and traffic congestion due to snow accumulation. Moreover, the minimum switching time is set to $T_{\text{mini}} = 10$ [min], considering the influence of frequent switching on the power distribution system.

B. Time Series Data for Simulation

In this section, we describe the acquisition and processing of actual time series data on electricity and weather used in the simulations of this chapter.

TABLE I
REFERENCE VALUES OF VOLTAGE PROFILE [15]

Parameter	Symbol	Value
Apparent power	W_{base}	10 [kVA]
Length of underground power distribution line	L_f	100 [m]
Voltage phase of underground power distribution line	θ_1	0 [rad]
Voltage amplitude of underground power distribution line	v_1	$\frac{6600}{\sqrt{3}}$ [V]
Voltage amplitude of heating cable	$\frac{1}{a_1}v_1$	200 [V]
Transformer ratio	a_1	$\frac{33}{\sqrt{3}}$
Conductance	g_{base}	918 [m/Ω]
Susceptance	b_{base}	918 [m/Ω]

TABLE II
P.U. VALUES OF VOLTAGE PROFILE [15]

Parameter	Symbol	p.u. value
Underground power distribution line		
Length	L_f	1
Voltage amplitude	v_1	1
Conductance	g_e	1
Susceptance	b_e	1
Heating cable		
Length	L_f	1
Conductance	g_h	0.5
Susceptance	b_h	0.5
Active power of load	$p_h(x_{\text{load}}, t)$	-10

1) *Power consumption and PV electric power generation:* The time series data on the power consumption of the residential loads are provided by Nagoya University Open Data for EMS Evaluation [16] for ten residential houses. As we consider only single phase of the three-phase underground distribution line, 1/3 of the time series data for 10 houses is used as the active power $p_e(x, t)$ of the residential load.

We use time series data of PV electric power generation provided by Hokuriku Electric Power Transmission and Distribution Company [17]. We also use the value that is $\frac{1}{1000}$ of the data in order to fit our data to the scale of the underground power distribution line considered in this paper. Furthermore, as we consider only one phase among the three phases, we use 1/3 of the time series data that fits the scale of the distribution system considered in this paper as the effective power $p_e(x, t)$ of the PV power generation equipment. On the other hand, when the power electricity is transmitted from the PV power generation equipment to the battery storage, we suppose that all the power electricity is transmitted. For this reason, we do not modify the scale of the data which is fit to the scale considered in this paper.

The power supplied by the PV electric power generation is considered to be more accurately predicted based on the day's weather forecast, compared to the power consumption of the load. Thus, we use the time series data for PV electric power generation as predictive data. In general, it is not easy to predict these data exactly. For this reason, the predicted value of the data at the predictive horizon continues to use

TABLE III
PARAMETERS RELATED TO HEATING CABLE, THERMAL DIFFUSION, AND SNOWMELTING [14]

Parameter	Symbol	Value
Heating cable		
Radiative cooling	q_r	0 [W/cm]
Contact heat transfer coefficient per unit length	γ_{cable}	1.04 [W/m·K]
Heat capacity	C_{cable}	18 [J/cm·°C]
Thermal conductivity of soil	λ_{soil}	0.5 [W/m·K]
Heat transfer coefficient between heating cable and soil	β_{cable}	300 [W/m ² ·K]
Thermal diffusion		
Burial depth of heating cable	D_f	10 [cm]
Thermal diffusivity of soil	α_{soil}	0.008 [m ² /s]
Heat transfer coefficient between ground surface and snow	β_{ground}	88 [W/m ² ·K]
Snowmelting		
Snow temperature	δ_{snow}	0 [°C]
Initial condition for snow volume	$h_{\text{snow}}(x, 0)$	30 [mm]
Unit conversion factor	a_{snow}	1.792×10^{-4}
Density of snow volume	d_{snow}	0.06 [g/cm ³]

TABLE IV
PARAMETERS RELATED TO EVALUATION FUNCTION

Parameter	Symbol	Value
Minimum switching time	T_{mini}	10 [min]
Predictive horizon	T_{pred}	30 [min]
Weighting coefficients (Heating cable)		
Distribution loss	w_{loss}	4×10^2
Voltage fluctuation	w_{fluc}	1×10^7
Snow volume	w_{snow}	1.2×10^5
Cost	w_{cost}	8×10^5
Weighting coefficients (PV)		
Voltage fluctuation	w_{pvfluc}	1
Amount of power of battery storage	$w_{\text{stor},1}$	1×10^{-3}
Weighting coefficients (Battery storage)		
Voltage fluctuation	$w_{\text{batteryfluc}}$	1
Amount of power of battery storage	$w_{\text{stor},2}$	1×10^{-3}

the value at the current time as a constant value in the computation of the evaluation function.

2) *Weather:* As the time series data of solar radiation, we use the average data of the radiation from 1981 to 2009 provided by NEDO's database viewing system [18]. Since this data is time series data at 1 h intervals, it is linearly interpolated as data at 30 sec intervals. Moreover, we choose the time series data observed in Toyama City. The data is provided by the Japan Meteorological Agency [19] for atmospheric temperature and wind speed. Since this data is given as time series data every 10 min, linear interpolation is performed to obtain data every 30 sec.

C. Case 1 (Morning without snowfall)

1) *Setting and time series data:* In this subsection, we consider a numerical simulation for a sunny winter morning with no snowfall from A.M. 6:00 to 8:00. This implies that that A.M. 6:00 and 8:00 correspond to $t = 0$ [min] and

$t = 120$ [min], respectively. For the time series data used in this case, we use January 19, 2016 for the residential load [16], January 19, 2020 for the PV electric power generation [17]. Fig. 5 shows the temporal variation of the power consumption of residential loads and PV electric power generation. We also use the time series data for atmospheric temperature [19], wind speed [19], and the average data from January 19, 1981 to 2009 for solar radiation [18]. The time series data on these quantities are shown in Fig. 6.

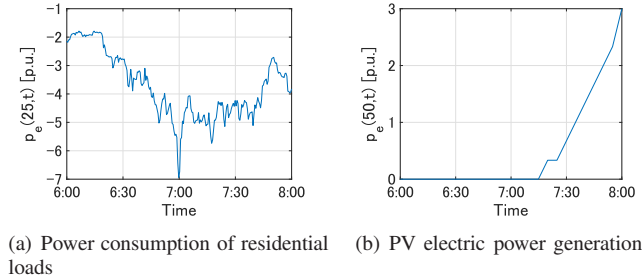


Fig. 5. Temporal variation of active powers (Case 1)

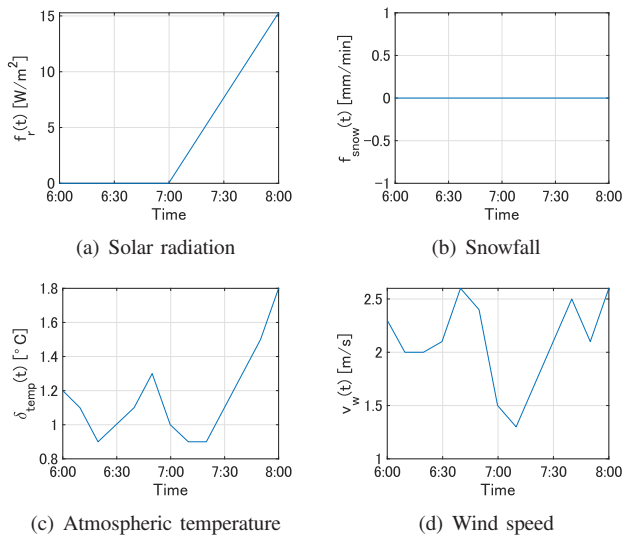


Fig. 6. Temporal variation of variables related to weather (Case 1)

2) Simulation result:

a) Temporal variation of variables: We show the simulation results for Case 1 in Fig. 7. In Fig. 7 (a), the voltage amplitude $v_e(x; t)$ [V] of the underground power distribution line varies as power consumption of the residential load and heating cable, and power supply from PV. The amplitude is reduced due to the power consumption of the residential load during A.M. 6:50 to 7:00. On the other hand, the amplitude increases with the PV electric power generation between A.M. 7:50 and 8:00. Fig. 7 (b) shows that the voltage amplitude $v_h(x; t)$ [V] of the heating cable varies greatly as the switches change. When Switch 1 is turned On, the voltage amplitude decreases from $x = 0$ [m] to $x = 100$ [m]. On the other hand, the amplitude decreases

from $x = 100$ [m] to $x = 0$ [m] during Switch 2 is turned On.

The temperature $\delta_{\text{surf}}(t; x)$ [°C] of the cable surface is shown in Fig. 7 (c). The temperature increases because Switches 1 or 2 are turned On from A.M. 6:00 to 7:30, and decreases during A.M. 7:30 to 8:00 when both switches are turned Off. When Switch 1 is turned On, the temperature at $x = 0$ [m] is higher than at $x = 100$ [m]. On the other hand, if Switch 2 is turned On, the temperature at $x = 100$ [m] increases compared to the temperature at $x = 0$ [m]. From Fig. 7 (d), the snow volume $h_{\text{snow}}(t; x)$ [mm] decreases with time.

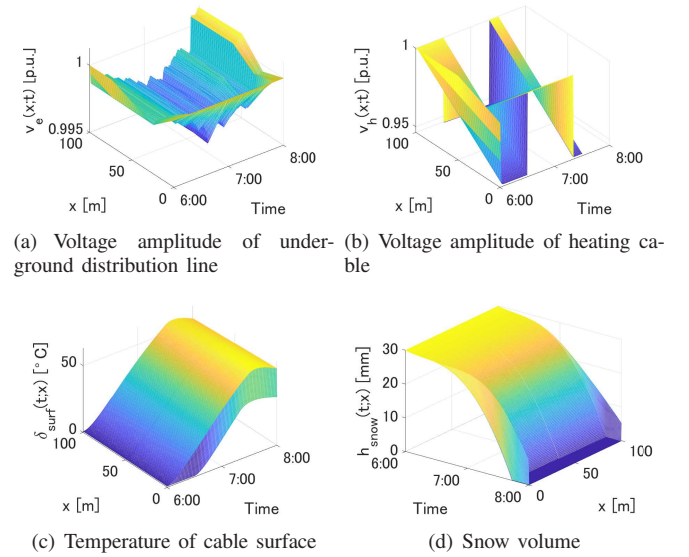


Fig. 7. Spatial and temporal variation of the variables (Case 1)

b) Temporal variation of switching and discharging: We show the simulation results for switching, and the PV power generation equipment, battery storage in Fig. 8.

Fig. 8 (a) illustrates the temporal variation of the switching control input for Case 1 by showing the index i which satisfies $\sigma_i(t) = 1$, the switch that turns On. From A.M. 6:00 to A.M. 6:30, Switch 2, which is powered by a battery storage, is turned to On. It is assumed that the owners of the heating cable and battery storage are the same, and Switch 2 is selected because it is less expensive than Switch 1. From A.M. 6:30 to 7:20, Switch 1 is set to On to melt snow, because the selection of Switch 2 would violate the constraint on the reserve capacity of the battery storage. From A.M. 7:20 to 7:30, Switch 2 is used for snow melting because the PV power generation system has supplied power to the battery storage. From A.M. 7:30 a.m. to 8:00, the switch is set to Off because the snow melting is almost completed.

Next, we show the temporal variation of the control input $\sigma_{\text{pv}}(t)$ of the PV power generation equipment in Fig. 8 (b). It can be confirmed that the power electricity is transmitted to the battery storage from A.M. 6:00 to 7:20 and from A.M. 7:40 to 7:50, and to the underground power

distribution line from A.M. 7:20 to 7:40 and from A.M. 7:50 to 8:00.

Finally, we show the temporal variation of the index i satisfying $\sigma_{\text{battery},i}(t) = 1$, i.e. the destination of the power electricity of the battery storage in Fig. 8 (c). When Switch 2 is turned On, the battery storage always transmits the power electricity to the heating cable. In addition, from A.M. 6:30 to 7:20 and from A.M. 7:30 to 8:00, the power electricity is stored to the battery without being transmitted anywhere. We also present the temporal variation of the amount of electricity in the battery storage in Fig. 8 (d). From A.M. 6:00 a.m. to 6:30 and from A.M. 7:20 a.m. to 7:30, the amount of power electricity decreases with time because the battery storage transmits power to the heating cables. From A.M. 7:10 to 7:20 a.m. and from A.M. 7:40 to 7:50 a.m., the amount of power electricity increases because the PV power generation equipment transmits power while the battery storage is not transmitting power electricity anywhere.

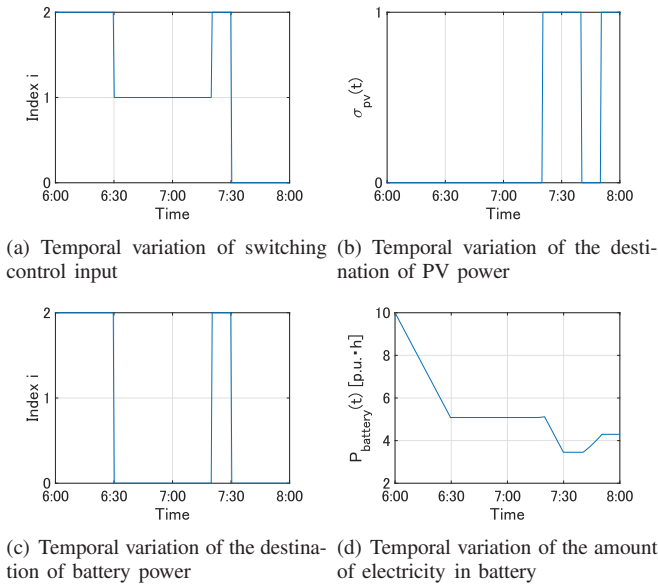


Fig. 8. Temporal variation with respect to switches, PV, and battery storage (Case 1)

c) Comparison with and without battery storage: In the following, we compare the cost and voltage variations without and with battery storage. Note that the former and latter simulations correspond to the result of the switching control due to the authors' previous study [9] and this paper, respectively.

We show the temporal variation of the switches for the cases without and with the battery storage in Fig. 9 (a) and Fig. 9 (b), respectively. In Fig. 9 (a), 15 [p.u.·h] of electricity is purchased because Switch 1 is selected from A.M. 6:00 am to 7:30. On the other hand, in Fig. 9 (b), Switch 1 is selected from A.M. 6:30 to 7:20, and thus 8.3 [p.u.·h] of electricity is purchased. Thus, with the introduction of the battery storage, we can confirm that the cost of using the heating cables is reduced.

Figs. 9 (c) and (d) show the temporal variation of the

voltage fluctuation of the underground power distribution line without and with the battery storage, respectively. Comparing the temporal variations for each case, there is no significant difference between the two cases. In Fig. 9 (c), if no battery storage is installed, the PV power generation equipment transmits all the power electricity to the underground power distribution line. On the other hand, in Fig. 9 (d), the equipment transmits power to the underground power distribution line and the battery storage. This shows the fact that the installation of the storage efficiently suppresses the voltage fluctuations while recharging the power, which implies the efficiency of the switching control of this paper comparing with [9].

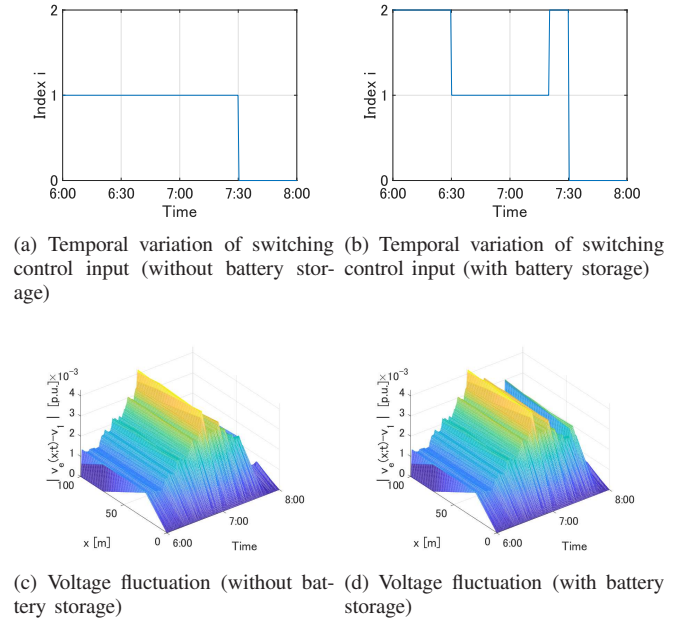
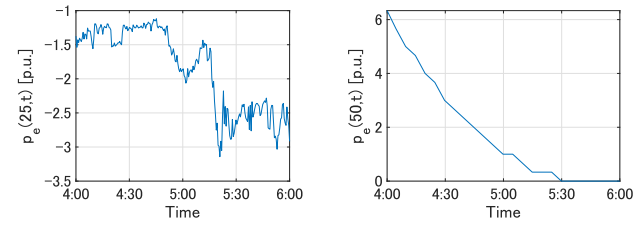


Fig. 9. Comparison of switching control input and voltage fluctuation with respect to battery storage (Case 1)

D. Case 2 (Evening with snowfall)

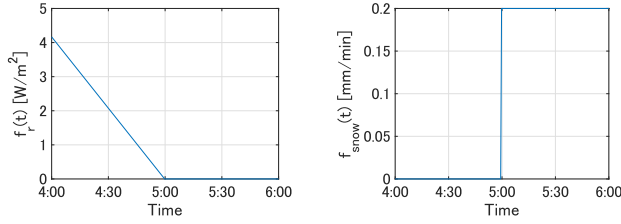
1) Setting and time series data: In this subsection, we consider a numerical simulation for a winter evening from P.M. 4:00 to 6:00 with snowfall starting from P.M. 5:00. This implies that P.M. 4:00 and 6:00 correspond to $t = 0$ [min] and $t = 120$ [min], respectively. We use the time series data of the residential load [16] from February 7, 2016, and of the PV electric power generation [17] from February 7, 2020. The temporal variation of the power consumption of residential load and PV electric power generation is shown in Fig. 10. The time series data for atmospheric temperature and wind speed are from February 7, 2020 [19]. Moreover, we choose the average solar radiation data from February 7, 1981 to 2009 [18]. The snowfall time series data gives a hypothetical snowfall of 12 mm per 1 hour assumed for Toyama Prefecture. The time series data of physical quantities related to weather are shown in Fig. 11.

2) Simulation result:

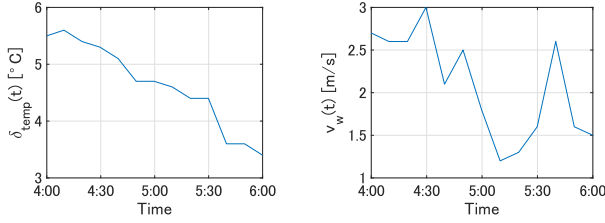


(a) Power consumption of residential loads (b) PV electric power generation

Fig. 10. Temporal variation of active powers (Case 2)



(a) Solar radiation (b) Snowfall



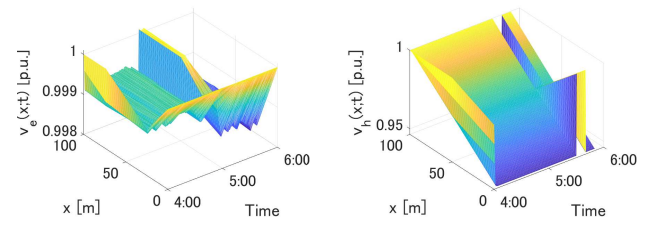
(c) Atmospheric temperature (d) Wind speed

Fig. 11. Temporal variation of variables related to weather (Case 2)

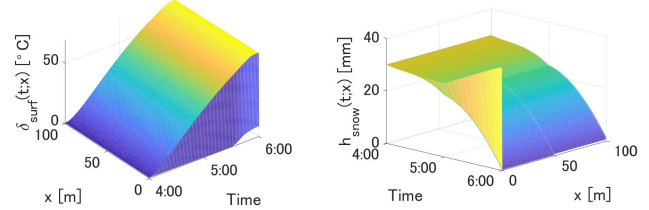
a) Temporal variation of variables: The simulation results for Case 2 are shown in Fig. 12. We show the temporal and spatial variations of the voltage amplitude of the underground distribution line in Fig. 12 (a). In this figure, the voltage fluctuation is suppressed by the power supplied by the PV power generation equipment against the increase of power consumption by the residential load from P.M. 5:00 to 5:30. In Fig. 12 (b), the voltage amplitude of the heating cable decreases from $x = 100$ [m] to $x = 0$ [m] because Switch 2 is set to On at many time intervals.

We show the temporal and spatial variations of the outer surface temperature $\delta_{\text{surf}}(t; x)$ [°C] of the heating cable in Fig. 12 (c). As for the temperature at $x = 100$ [m], the temperature at $x = 0$ [m] is higher than that at $x = 0$ [m], because Switch 2 is set to On during many time periods. Moreover, in Fig. 12 (d), The occurrence of snowfall from P.M. 5:00 has changed the decrease of the snow accumulation $h_{\text{snow}}(t; x)$ [mm].

b) Temporal variation of switching and discharging: We show the simulation results for the switches, the PV power generation equipment, and the battery storage in Fig. 13. The temporal variation of the switching of the switch with subscript i , i.e., On, satisfying $\sigma_{b,i}(t) = 1$ is shown in Fig. 13 (a). From P.M. 4:00 to 5:30, Switch 2, which is



(a) Voltage amplitude of underground distribution line (b) Voltage amplitude of heating cable



(c) Temperature of cable surface (d) Snow volume

Fig. 12. Spatial and temporal variation of the variables (Case 2)

powered by a battery storage, is set to On. Since the owners of the heating cables and the battery storage are supposed to be the same, we can conclude that Switch 2 is chosen because it is less expensive than Switch 1, which is set to On. From P.M. 5:30 to 5:40, Switch 1 is set to On. This is considered to be to promote the snow melting at the starting point $x = 0$ [m]. Then, from P.M. 5:50 to 6:00, the switch is set to Off because the snow melting is almost completed.

We show the temporal variation of the control input $\sigma_{\text{PV}}(t)$ of the PV power generation equipment in Fig. 13 (b). In the time interval from P.M. 5:00 to 5:30, the equipment transmits power to the underground power distribution line. The reason for this is considered to be the increase in the power consumption of residential loads during this interval. Moreover, Fig. 13 (c) shows the temporal variation of the subscript i satisfying $\sigma_{\text{battery},i}(t) = 1$, i.e., the destination of the power from the battery storage. When Switch 2 is set to On, the storage always transmits the power to the heating cable.

The temporal variation of the amount of power electricity stored in the battery storage is shown in Fig. 13 (d). The initial amount of the power electricity in the battery storage is assumed to be 10 [p.u.h]. From P.M. 4:00 to 4:30, the amount of the power electricity stored in the battery storage is increasing because the amount of the power electricity transmitted from the PV power generation equipment is larger than the amount of the electricity transmitted to the heating cable. However, from P.M. 4:30 p.m. to 5:30, the amount of the power electricity transmitted from the PV power generation equipment gradually decreases, and the amount of the power electricity in the battery storage also decreases.

c) Comparison with and without battery storage: In the following, we compare the costs and the voltage fluctuations with and without battery storage. Similarly to Case 1, the

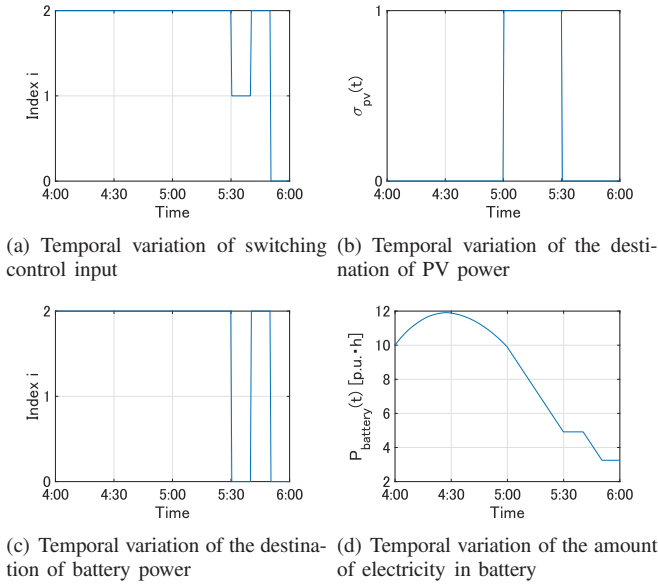


Fig. 13. Temporal variation with respect to switches, PV, and battery storage (Case 2)

former and latter simulations correspond to the authors' previous study [9] and this paper, respectively.

Fig. 14 (a) shows the switching when no battery storage is installed, and Fig. 14 (b) shows the switching when a battery storage is installed. If no battery storage is installed, Switch 1 is selected between P.M. 4:00 and 5:40, and thus 16.7 [p.u.·h] of the power electricity is purchased. On the other hand, when the battery storage is installed, Switch 1 is selected from P.M. 5:30 to 5:40, and thus 1.7 [p.u.·h] of the power electricity is purchased. We can confirm that the introduction of the storage has significantly reduced the cost of using the heating cables.

Figs. 14 (c) and (d) show the voltage fluctuations without and with battery storage, respectively. From these figures, it can be confirmed that the voltage fluctuations are more suppressed when the battery storage is installed. This is because the battery storage optimizes the power flow according to the power consumption of the house and the amount of the PV power generation.

V. CONCLUSIONS

In this paper, we have studied the application of a battery storage to the predictive switching control of a power distribution system including road heating proposed by the authors [9]. The introduction of a battery storage increases the number of transmission destinations of power electricity from the PV generation equipment, and improves the power flow in terms of optimization. The predictive switching control is designed for the PV power generation equipment and the battery storage, respectively. Its effectiveness is demonstrated by numerical simulations using the actual time-series data. As a conclusion, we have confirmed the effectiveness of the introduction of battery storage compared to the authors' previous study [9].

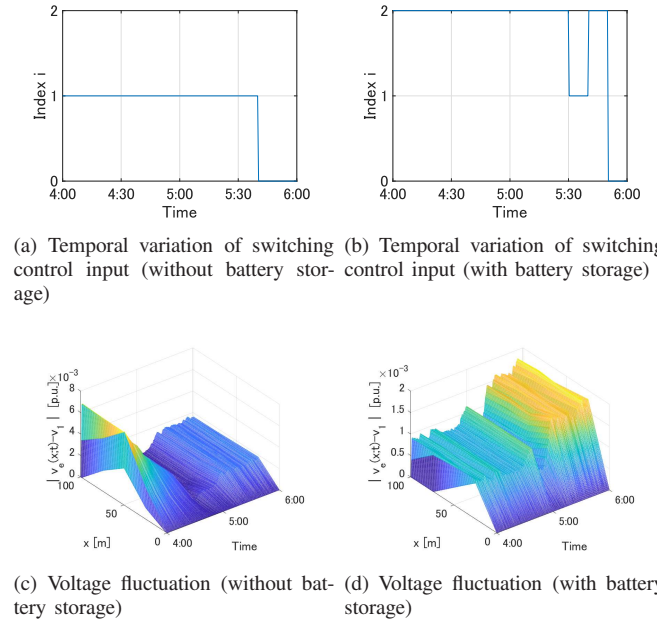


Fig. 14. Comparison of switching control input and voltage fluctuation with respect to battery storage (Case 2)

As a future work, in order to improve the control performance of the switching predictive control, it is necessary to add constraints on the voltage amplitude and to consider the weights of the evaluation function according to the distribution system and its specific situation.

REFERENCES

- [1] W. J. Eugster: *Road and bridge heating using geothermal energy- Overview and examples*, Proceedings European Geothermal Congress 2007, 2007.
- [2] W.B. Yu, X. Yi, M. Guo, and L. Chen: *State of the art and practice of pavement anti-icing and de-icing techniques*, Sciences in Cold and Arid Regions, **60**(2014), 14-21.
- [3] R. Merrifield: *Under-road heating system to keep Europe's highways ice-free*, Horizon: The EU Research and Innovation Magazine, European Commission, 2019.
- [4] W.H. Kersting: *Distribution system modeling and analysis*, Fourth edition, Routledge, 2018.
- [5] P.S. Kundur: *Power system stability and control*, McGraw Hill, 1994.
- [6] Y. Muto, C. Kojima, and Y. Okura: *Mathematical modeling of road heating system with underground distribution line based on nonlinear ODE model*, Nonlinear Theory and Its Applications, IEICE, **14**(2023), 378-402.
- [7] M. Chertkov, S. Backhaus, K. Turtisyn, V. Chernyak, and V. Lebedev: *Voltage collapse and ODE approach to power flows: Analysis of a feeder line with static disorder in consumption/production*, arXiv, 2011, 1106.5003.
- [8] H. Tadano, Y. Susuki, and A. Ishigame: *Asymptotic assessment of distribution voltage profile using a nonlinear ODE model*, Nonlinear Theory and Its Applications, IEICE, **13**(2022), 149-168.
- [9] Y. Muto, C. Kojima, and Y. Susuki: *Switching Predictive Control of Power Distribution System Including Road Heating*, Transactions of the Society of Instrument and Control Engineers, **60**(2024), 384-396 (in Japanese).
- [10] H. Sugihara, T. Funaki, and N. Yamaguchi: *Evaluation method for real-time dynamic line ratings based on line current variation model for representing forecast error of intermittent renewable generation*, Energies, **10**(2017), 503.
- [11] A. Inomata, R. Hara, T. Oyama, and I. Kurihara: *Effectiveness of application of dynamic rating to transmission system*, IEEE Transactions on Power and Energy, **126**(2006), 36-42 (in Japanese).

- [12] C. Kojima, Y. Muto, and Y. Susuki: *On dissipativity of nonlinear ODE model of distribution voltage profile*, Proceedings of IFAC World Congress 2023, 2023, 7031-7036.
- [13] I. Gushiken and N. Tosaka: *Boundary element analysis of 1-D unsteady thermal convection problem*, Transactions of Boundary Element Method, Japan Society for Computational Methods in Engineering, **19**(2002).
- [14] H. Takimoto, A. Ogura, M. Yoshida, K. Takase, and T. Maruyama: *Analysis of snowpack accumulation and melting with a heat balance approach - Role of heat flux from underground in melting snow*, Transactions of The Japanese Society of Irrigation, Drainage and Rural Engineering, **82**(2014) 191-200 (in Japanese).
- [15] Y. Susuki, S. Baek, Y. Ota, and T. Hikiyama: *Computer Simulation of Distribution Voltage Profile Using a Nonlinear ODE*, IEICE Technical Report, **116**(2016) (in Japanese).
- [16] Nagoya University, *Nagoya University Open Data for EMS Evaluation*, 2023 (in Japanese). <http://data.v2x-ems.nagoya/down/sample>
- [17] Hokuriku Electric Power Transmission and Distribution Company: *Hokuriku Area Electricity Forecast*, 2022 (in Japanese). <https://www.rikuden.co.jp/nw/denki-yoho/>
- [18] NEDO: *Database for Solar Radiation*, 2017 (in Japanese). <https://appww2.infoc.nedo.go.jp/appww/index.html>
- [19] Japan Meteorological Agency: *Historical Data Search*, 2023 (in Japanese). <https://www.data.jma.go.jp/obd/stats/etrn/index.php>